Quantitative Changes in *Gimap3* and *Gimap5* Expression Modify Mitochondrial DNA Segregation in Mice

Riikka Jokinen,* Taina Lahtinen,* Paula Marttinen,* Maarit Myöhänen,* Pilvi Ruotsalainen,* Nicolas Yeung,* Antonina Shvetsova,† Alexander J. Kastaniotis,† J. Kalervo Hiltunen,† Tiina Öhman,‡ Tuula A. Nyman,‡ Hartmut Weiler,§ and Brendan J. Battersby*,[1]

*Research Programs Unit—Molecular Neurology, Biomedicum Helsinki, and ‡Institute of Biotechnology, University of Helsinki, 00290 Helsinki, Finland, †Department of Biochemistry and Biocenter Oulu, University of Oulu, 90014 Oulu, Finland, and §Blood Research Institute, Blood Center of Wisconsin, Milwaukee, Wisconsin 53266

ABSTRACT Mammalian mitochondrial DNA (mtDNA) is a high-copy maternally inherited genome essential for aerobic energy metabolism. Mutations in mtDNA can lead to heteroplasmy, the co-occurence of two different mtDNA variants in the same cell, which can segregate in a tissue-specific manner affecting the onset and severity of mitochondrial dysfunction. To investigate mechanisms regulating mtDNA segregation we use a heteroplasmic mouse model with two polymorphic neutral mtDNA haplotypes (NZB and BALB) that displays tissue-specific and age-dependent selection for mtDNA haplotypes. In the hematopoietic compartment there is selection for the BALB mtDNA haplotype, a phenotype that can be modified by allelic variants of *Gimap3*. Gimap3 is a tail-anchored member of the GTPase of the immunity-associated protein (Gimap) family of protein scaffolds important for leukocyte development and survival. Here we show how the expression of two murine *Gimap3* alleles from *Mus musculus domesticus* and *M. m. castaneus* differentially affect mtDNA segregation. The *castaneus* allele has incorporated a uORF (upstream open reading frame) in-frame with the *Gimap3* mRNA that impairs translation and imparts a negative effect on the steady-state protein abundance. We found that quantitative changes in the expression of *Gimap3* and the paralogue *Gimap5*, which encodes a lysosomal protein, affect mtDNA segregation in the mouse hematopoietic tissues. We also show that Gimap3 localizes to the endoplasmic reticulum and not mitochondria as previously reported. Collectively these data show that the abundance of protein scaffolds on the endoplasmic reticulum and lysosomes are important to the segregation of the mitochondrial genome in the mouse hematopoietic compartment.

KEYWORDS mitochondria; mitochondrial DNA; mice; segregation; Gimap

MAMMALIAN mitochondrial DNA (mtDNA) is a maternally inherited small circular multicopy genome that encodes 13 proteins that are essential subunits of four of the five complexes required for mitochondrial oxidative phosphorylation. Germline or somatic-cell mtDNA mutations lead to the co-occurrence of two or more sequence variants in a cell, a state known as heteroplasmy. In the absence of selection, the segregation of mtDNA sequence variants is neutral and can be modeled as a random walk (Chinnery and Samuels 1999); however, in some cases there is preferential selection for a mtDNA sequence variant that is dependent upon the nucleotide sequence, tissue, and nuclear background (Battersby and Shoubridge 2001; Battersby *et al.* 2003, 2005; Jokinen and Battersby 2013; Burgstaller *et al.* 2014). The majority of pathogenic mtDNA mutations are heteroplasmic and some mutations display skewed segregation patterns in somatic tissues. (Larsson *et al.* 1990; Boulet *et al.* 1992; Kawakami *et al.* 1994; Dunbar *et al.* 1995; Fu *et al.* 1996; Chinnery *et al.* 1997, 1999; Weber *et al.* 1997), which can affect the onset and severity of mitochondrial dysfunction. Currently, the molecular basis for this regulation of the mitochondrial genome is largely unknown (Jokinen and Battersby 2013).

To study mtDNA segregation in mammals we use a heteroplasmic mouse model with two neutral mtDNA variants

Copyright © 2015 by the Genetics Society of America
doi: 10.1534/genetics.115.175596
Manuscript received February 17, 2015; accepted for publication March 20, 2015; published Early Online March 25, 2015.
Supporting information is available online at http://www.genetics.org/lookup/suppl/doi:10.1534/genetics.115.175596/-/DC1.
[1]Corresponding author: Research Programs Unit, Molecular Neurology, r. C524b, Biomedicum Helsinki, University of Helsinki, Haartmaninkatu 8, 00290 Helsinki, Finland. E-mail: brendan.battersby@helsinki.fi

derived from two old inbred mouse strains, BALB/c and NZB (Jenuth *et al.* 1996, 1997). These mtDNA haplotypes, referred to as BALB and NZB, differ at 90 nucleotide positions (Hagstrom *et al.* 2014) and have been stably transmitted through the female germline of this mouse model for ~20 years (Jenuth *et al.* 1996). There is no selection for either mtDNA haplotype during transmission as the heteroplasmy level in the offspring follows a Gaussian distribution (Jenuth *et al.* 1996; Wai *et al.* 2008). However, postnatally there is age-dependent selection of one haplotype over the other in three tissue types (liver, kidney, and hematopoietic tissues), while all other tissues in these mice are neutral with respect to mtDNA segregation (Jenuth *et al.* 1997). In the liver and kidney there is selection for the NZB haplotype to fixation (Jenuth *et al.* 1997; Battersby and Shoubridge 2001; Battersby *et al.* 2003, 2005). In contrast, the hematopoietic tissues (bone marrow, blood, thymus, and spleen) select against the NZB mtDNA haplotype, which can be modeled as an exponential decay (Battersby *et al.* 2005). This tissue-specific mtDNA segregation is best treated as a quantitative genetic phenotype and one that cannot be explained by detectable functional differences in the mitochondrial respiratory chain or by differential rates in mtDNA replication (Battersby and Shoubridge 2001).

To uncover the molecular basis of this mtDNA regulation we have used forward genetic approaches in mice. On the nuclear background of *M. m. domesticus* in several different mouse strains (BALB/c, C3H, C57BL/6J, DBA, NZB, and 129Sv) there are no differences in these tissue-specific mtDNA segregation phenotypes (Battersby *et al.* 2003, 2005). In contrast, crosses onto a *M. m. castaneus* nuclear background have a significant effect on these mtDNA segregation phenotypes (Battersby *et al.* 2003, 2005). This allowed us to identify three nuclear loci that affect mtDNA segregation in a tissue-specific manner (Battersby *et al.* 2003). At one of these loci we have successfully cloned *Gimap3* (Jokinen *et al.* 2010), which can modulate the segregation of mtDNA in leukocytes.

GTPase of the immunity-associated proteins (Gimap) are encoded in a conserved cluster of seven to eight genes found only in vertebrates with an ortholog in plants (Krucken *et al.* 2004). In mammals, *Gimap* expression appears to be restricted to hematopoietic tissues and is important for leukocyte development and survival, although the molecular basis for these functions is poorly understood (Krucken *et al.* 2004; Nitta and Takahama 2007; Schulteis *et al.* 2008; Barnes *et al.* 2010; Chen *et al.* 2011). Gimaps can be tail anchored or soluble and are structurally related to Septins, Tocs, and Dynamins (Schwefel *et al.* 2010). Based on structural studies the membrane anchored Gimaps form GTP-dependent homooligomers with low inherent GTP hydrolysis activity that stabilizes these oligomers allowing them to act as scaffolds (Schwefel *et al.* 2010, 2013).

Gimap3 and *Gimap5* are paralogues in this gene cluster and 84% identical at the amino acid level, differing only at the N and C termini (Krucken *et al.* 2004). Both have a short transmembrane domain at the C terminus for insertion into a lipid bilayer. The intracellular localization of Gimap5 has been controversial with data reporting insertion into many different organelles. However, data using species-specific monoclonal antibodies against Gimap5 in T cells robustly demonstrate that in humans, mice, and rats the protein is anchored into the lysosomal membrane (Wong *et al.* 2010). So far there is only one report for the localization of Gimap3 suggesting it is mitochondrial (Daheron *et al.* 2001). In mice, both genes are expressed and appear to be important for T-cell development (Nitta *et al.* 2006) and possibly in a cooperative way (Yano *et al.* 2014). In contrast, *GIMAP3* in humans appears to be a pseudogene (Krucken *et al.* 2004). Complete loss of *Gimap5* function in mice appears to be catastrophic for the hematopoietic compartment, producing a decrease of lineage-committed hematopoietic progenitors leading to a reduction of T and B lymphocytes, NK and NK T cells, altered erythropoiesis, and early lethality (Schulteis *et al.* 2008; Barnes *et al.* 2010; Chen *et al.* 2011). In rats the loss of Gimap5 function is milder, as a premature termination in *Gimap5* of the BioBreeding rat results only in a T-cell lymphopenia, which is a susceptibility factor for autoimmunity in this diabetic rodent model (Hornum *et al.* 2002; MacMurray *et al.* 2002). Both Gimap3 and Gimap5 have been shown to interact with Bcl2 family members (Nitta *et al.* 2006; Chen *et al.* 2011), although the function of these interactions on membrane surfaces has yet to be elucidated.

Here, we investigated in more detail the basis by which *Gimap3* is important for mtDNA segregation in the mouse hematopoietic compartment. We show that the tail-anchor sequence of Gimap3 localizes the protein to the endoplasmic reticulum (ER) and not the mitochondrial outer membrane as previously reported. The steady-state abundance of Gimap3 in leukocytes appears to be a critical factor for the regulation of mtDNA segregation in mouse hematopoietic tissues. Our data also implicate a role for the paralogue *Gimap5* in mtDNA segregation. Together our findings demonstrate that the abundance of two membrane-bound protein scaffolds on the endoplasmic reticulum and lysosomes are important modulators to the segregation of the mitochondrial genome in mouse leukocytes.

Materials and Methods

Animals

The Regional State Administrative Agency of Southern Finland (ESAVI) approved all mouse work. The *Gimap5*^{tm1Wlr} knockout mouse and the heteroplasmic mice were maintained on the BALB/c nuclear background and housed under standard conditions applied by the University of Helsinki Laboratory Animal Center. The animals in experiments were housed and sampled in random groups. Both male and female mice were used in the analyses.

Cell culture

Cells (murine embryonic fibroblasts, COS7, NIH3T3) were cultured under standard conditions (DMEM, 10% fetal bovine serum, glutamax). Splenocytes were freshly isolated

from BALB/c mice (Battersby *et al.* 2005). MG132 (20 μM) (Sigma) was dissolved in DMSO.

cDNAs, plasmids, and retroviral expression

Full-length cDNAs (BALB *Gimap3*, BALB *Gimap5*, CAST *Gimap3*, BALB *Gimap3-omp25*, *YFP-Gimap3*, *YFP-(263-301) Gimap3*, *RFP-Gimap3*, pGFP-omp25 (Nemoto and De Camilli 1999) (gift from Hans Spelbrink) were cloned into Gateway (Invitrogen) converted retroviral expression vectors (pBABE-puro, pMYS-IRES-Neo, or pMXs-IRES-Blasticidin) or pcDNA3.1 for transient transfections. Retroviral vectors were transfected (Jetprime, Polyplus) into the Phoenix amphotropic packaging line for virus production to infect recipient cells (MEFs and COS-7). Following antibiotic selection, cells were used in experiments. For transient expression, plasmids were transfected (Jetprime, Polyplus) into COS-7 and HEK293 cells. The GFP–Sec61β plasmid was a gift from Benoit Kornmann).

Immunoblotting and antibodies

Cells or tissue samples were solubilized in phosphate buffered saline, 1% dodecyl-maltoside, 1 mM PMSF (phenylmethylsulfonyl fluoride), complete protease inhibitor (Roche). Protein concentrations were measured by the Bradford assay (Bio-Rad). Equal amounts of proteins were separated by Tris-glycine SDS–PAGE and transferred to nitrocellulose by semi-dry transfer. Primary antibodies were incubated overnight at +4° and detected the following day with secondary HRP conjugates (Jackson ImmunoResearch) using enhanced chemiluminescence (Cell Signaling) with film or a Bio-Rad chemi-doc imaging station. Gimap3 antibodies were generated in rabbits with the following peptides: BALB variant, amino acids 2–16 (ETLQNVVTGGKKGGC) and amino acids 259–272 (C-EGSWVLKVLPIGKK) and CAST variant, amino acids 32–45 (RIPVYTTDHLRCPDS). Sources for commercial antibodies: Chromotek (anti-GFP); Mitosciences (Sdha); Millipore (Porin); Proteintech Group (Atp5B, Calnexin, and RPL18a); Sigma (anti-HA and Atg5), Santa Cruz (Tom40). Representative immunoblotting data from multiple independent biological experiments were cropped in Photoshop with only linear corrections applied. When quantified, Western blots were analyzed with Bio-Rad chemi-doc imaging station and Image Lab software.

In vitro protein synthesis

Proteins were synthesized with TNT T7-coupled reticulocyte lysate system (Promega) according to manufacturer's instructions using plasmids with Gimap3 or YFP cDNA constructs cloned into pcDNA3.1. Each reaction also included Superase RNAse inhibitor (Ambion) and [^{35}S]Met-Cys (EasyTag, Perkin Elmer) and incubated for 25 min at 30°. The reaction time was chosen based upon linear radiolabel incorporation for YFP (Figure S2). Equal aliquots from each reaction mix were separated by SDS–PAGE with the gel dried and exposed to a Phosphoscreen for scanning with a Typhoon 9400 (GE Healthcare) for quantification.

Histodenz gradients

Mouse spleens were homogenized in buffer (200 mM mannitol, 70 mM sucrose, 10 mM HEPES, 1 mM EGTA pH 7.5) with a Teflon pestle and then centrifuged twice at 600 × *g* for 10 min. The post-nuclear suspension was mixed with an equal volume of 50% Histodenz (Sigma) (10 mM HEPES, 1 mM EGTA pH 7.5). A discontinuous Histodenz gradient was then formed (10, 15, 20, 25, and 30%) to separate organelles (Okado-Matsumoto and Fridovich 2001). Samples were centrifuged in a SW32.1Ti rotor for 90 min at 52 000 × *g* at +4°. Fractions were collected from the top, precipitated with TCA, and then resuspended in 1× Laemmli buffer. Samples were then subjected to SDS–PAGE and immunoblotting.

Sucrose gradient centrifugation

HEK293 cells from a 150-mm plate were treated with 100 μg/ml cycloheximide upon harvesting and lysed in 450 μl of lysis buffer (20 mM Tris-HCl pH 7.5, 150 mM NaCl, 5 mM $MgCl_2$, 1 mM DTT, 100 μg/ml cycloheximide, 1% Triton X-100) with Superase RNAse inhibitor (Ambion) for 20 min and centrifuged for 5 min at 13,000 × *g* at 4°. The supernatant was loaded on a 16-ml linear 10–50% sucrose gradient (20 mM HEPES pH 7.6, 100 mM KCl, 5 mM $MgCl_2$) and centrifuged for 200 min at 28,000 rpm at 4° (Beckman, SW 32.1 Ti). Eighty-two equal volume (200 μl) fractions were collected from the top. A total of 100 μl of each fraction was used for measuring RNA absorbance at 254 nm. The remaining fractions were pooled, combining five consecutive fractions, for TCA precipitation, heated at 95° for 5 min and separated by 12% SDS–PAGE for immunoblotting.

Mitochondrial DNA analysis

All sampled mouse tissues were immediately frozen in liquid nitrogen and stored at −80°. Total DNA was extracted with phenolchloroform and mtDNA heteroplasmy level determined as described in Battersby and Shoubridge (2001). Modeling selection for mtDNA in the hematopoietic tissues of heteroplasmic mice was as described in Battersby *et al.* (2005). Data sets were tested first for normality then subject to parametric statistics (two-tailed *t*-test).

RNA analysis

All tissues sampled were frozen in liquid nitrogen and stored at −80°. Total RNA was extracted with Trizol (Invitrogen) then treated with DNaseI to eliminate potential DNA contamination. Allelic expression of *Gimap3* was measured from total RNA amplified by semiquantitative RT–PCR compared to a standard curve with equimolar mixtures of CAST/Ei and BALB/c RNA (r^2 = 0.97) and quantified with a Typhoon 9400. Data were analyzed statistically using a Mann–Whitney *U*-test.

For Northern blotting total RNA was isolated from frozen spleens and thymi homogenized in Trizol (Invitrogen) with Precellys 24 tissue homogenizer (Bertin technologies) with mixed beads and a homogenization cycle of 5500 rpm for

25 sec. Total RNA was isolated by Trizol from stable retroviral cell line controls and treated with DNaseI (New England Biolabs). A total of 15 μg of RNA for tissue samples and 5 μg for the cell line controls (concentration determined with a Nanodrop1000 spectrophotometer) were separated on a 1.2% agarose–formaldehyde gel and transferred by neutral transfer to Hybond-N^+ membrane (GE healthcare). The membrane was UV cross-linked and consecutively probed with oligonucleotide probes for *Gimap3* and *Atp5B*. The probes were 5′ radiolabeled with T4 PNK (New England Biolabs) and purified with Illustra ProbeQuant G-50 micro-column (GE Healthcare). Hybridization (25% formamide, 7% SDS, 1% BSA, 0.25 M sodium phosphate pH 7.2, 1 mM EDTA pH 8.0, 0.25 M $NaCl_2$) was performed for 16–20 hr at 37°. Membranes were washed (2× SSC/0.1% SDS and 0.2× SSC/0.1% SDS) and then dried for exposure on Storage Phosphor screens (GE Healthcare), which were scanned and quantified with a Typhoon 9400 (Amersham).

Microscopy

Cells were grown on glass coverslips and fixed in fresh 4% paraformaldehyde. Coverslips were mounted with DABCO/MOWIOL on glass slides for imaging. Confocal images were taken on a Zeiss META 510 with the 63× Plan-Apochromat (1.4 NA) objective using the Argon (488 nm) and HeNe1 (543 nm) lasers or a Leica TCS Sp8 CARS with a 63× APO (1.2 NA) water objective using the Argon (488 nm) and DPSS (561 nm) lasers. Fluorescence microscopy was carried out on a Zeiss Axioplan2 using a 63× (1.25 NA) or 100× (1.3 NA) objective. Image processing and line profiles were performed using Image J. Only linear corrections were applied to images.

iTRAQ analysis

Three mouse spleens per genotype were homogenized (200 mM mannitol, 70 mM sucrose, 10 mM HEPES, 1 mM EGTA pH 7.5) with a Teflon pestle. Differential centrifugation was used to enrich for the membrane compartment containing Gimap3 and Gimap5. The postnuclear lysate (two 600 × *g* for 10 min) was first centrifuged at 5000 × *g* for 10 min and the resulting pellet was discarded. The supernatant was then centrifuged for 20 000 × *g* for 40 min. This pellet was solubilized and a total of 120 μg of protein per sample was precipitated using 2-D Clean Up Kit (GE Healthcare). The precipitated proteins were dissolved into 30 μl of iTRAQ dissolution buffer, and 2 μl of each sample was subjected to SDS–PAGE and silver staining to control for protein amount in the samples after precipitation. Protein alkylation, trypsin digestion and labeling of the resulting peptides were performed according to manufacturer's instructions (Applied Biosystems). After labeling, the samples were pooled and dried, and the peptides were fractionated by strong cation exchange chromatography using an Ettan HPLC system (Amersham Biosciences) connected to a Polysulfoethyl A column. Each selected SCX fraction containing labeled peptides was then processed with C18 Spin Columns (Pierce) according to the manufacturer instructions before being analyzed twice with nano-LC-ESI-MS/MS using Ultimate 3000 nano-LC (Dionex) and QStar Elite mass spectrometer (Applied Biosystems) as previously described (Lietzen *et al.* 2011). MS data were acquired automatically using Analyst QS 2.0 software. iTRAQ analyses were performed on three biological replicate samples.

Protein identification and relative quantitation were performed with Paragon search algorithm (Shilov *et al.* 2007) using ProteinPilot 4 interface (Applied Biosystems). Data files from both technical replicates of an iTRAQ sample set were processed together. Database searches were performed against mouse protein sequences in UniProt database (v. 2012-08-13 with 16 540 mouse entries). The search criteria were cysteine alkylation with MMTS, trypsin digestion, biological modifications allowed, thorough search and detected protein threshold of 95% confidence (Unused ProtScore >1.3). Additionally, automatic bias correction was used to correct for uneven protein loading. The false discovery rates were calculated as previously described (Elias and Gygi 2007) and were <1% for all biological replicates.

Relative quantity fold change of 0.66 or 1.5 was used as a threshold for changed proteins, and proteins were included in the data set only if they either exhibited similar change in at least two of the biological replicates, or a statistically significant quantitation change in one of the replicates and no changes in the others. Biological process for the identified proteins was retrieved from UniProtKB.

Results

Previously we identified *M. musculus* allelic variants of *Gimap3* that affect mtDNA segregation in hematopoietic tissues (Jokinen *et al.* 2010). In the common lab mouse strains with a *M. m. domesticus* background, such as BALB/c, *Gimap3* contains five exons and transcription produces an mRNA with two AUG codons as potential start codons for translation initiation (Figure 1A). The first AUG encodes an upstream open reading frame (uORF) of 60 amino acids, while translation initiation on the second AUG generates a 301-amino-acid protein (Figure 1A and Supporting Information, Figure S1) that contains the conserved GTPase domain that defines the Gimap family. Surprisingly, the uORF has a greater Kozak consensus sequence around the AUG than that seen for the downstream reading frame of Gimap3 (Figure 1B). Unless indicated otherwise, hereafter *Gimap3* refers to the allele found among the common lab strains with a *M. m. domesticus* background that encodes the 301-amino-acid protein (Jokinen *et al.* 2010). In contrast, the subspecies *M. m. castaneus* has a mutation in the splice acceptor site of exon 4 causing a splicing defect leading to the absence of exon 4 from the CAST *Gimap3* mRNA (Figure 1A) (Jokinen *et al.* 2010). In this CAST allele the AUG of the uORF is used for translation initiation producing a 359 amino acid protein (Figure 1A and Figure S1). These two allelic variants of Gimap3 are identical at the amino-acid-sequence level within

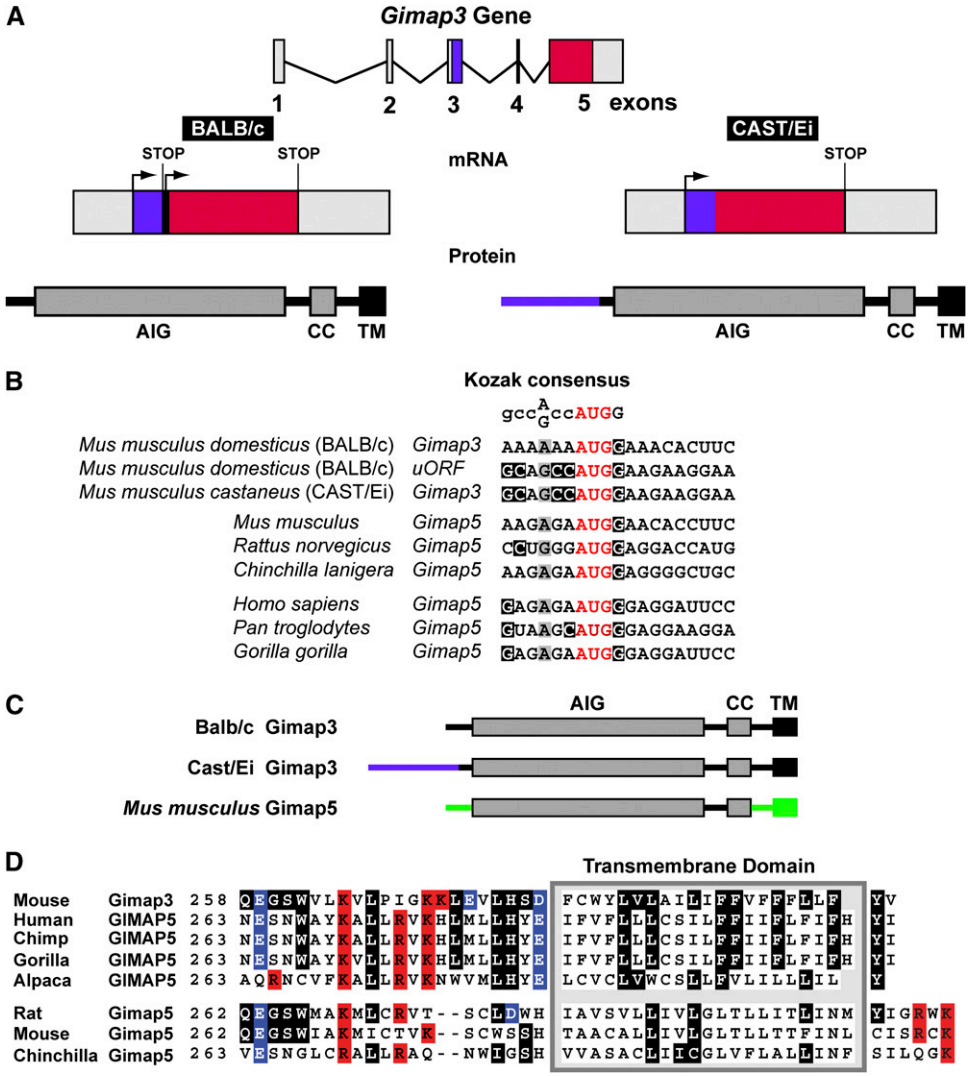

Figure 1 The organization of the *Gimap3* gene in mice. (A) A graphical illustration of the *Gimap3* gene, mRNA, and protein derived from BALB/c and CAST/Ei alleles. Red indicates the main coding sequence for Gimap3, while purple indicates the sequence of the uORF. CC, coiled coil; TM, transmembrane; AIG, Gimap family domain. (B) Alignment of the predicted starter methionine from *Gimap3* and *Gimap5* across selected mammalian taxa against the Kozak consensus sequence. (C) A graphical illustration of the Gimap3 and Gimap5 proteins with color differences indicating sequence divergence between the two proteins. (D) An amino acid alignment of the C terminus of Gimap3 against Gimap5 from selected mammalian taxa. Predicted transmembrane domain with flanking charged amino acids: positive in red and negative in blue. Amino acids in Gimap3 that are conserved with Gimap5 appear in white type on a black background.

all of the known functional domains and differ only at the N terminus, which has an additional 58 amino acids in the CAST/Ei version (Figure 1A) (Jokinen *et al.* 2010). Linkage mapping and transgenic expression of the CAST *Gimap3* cDNA established that this allele significantly decreases the rate of mtDNA segregation in the mouse hematopoietic compartment (Jokinen *et al.* 2010).

In the annotated genomes of most mammals *Gimap3* appears to be absent from the *Gimap* gene cluster. In humans, *GIMAP3* appears to be a pseudogene (Krucken *et al.* 2004) and it is not clear whether this gene function has been completely lost or taken over by *GIMAP5*. However, the high identity in nucleotide sequence between *Gimap3* and *Gimap5* can be a complicating factor in the robustness of the genome annotations with respect to the presence of *Gimap3* in these taxa. Thus, it is still an open question whether *Gimap3* is specific to mice. Aligning the C-terminal amino acid sequence of mouse Gimap3 against that of Gimap5 from a number of mammalian taxa demonstrates that the rodent Gimap5 possesses a difference in the charge balance around the tail-anchor sequence and in the amino acid composition of the transmembrane domain (Figure 1D). These features are critical for intracellular localization of tail-anchor proteins (Rapaport 2003). Based upon this protein alignment of the C terminus it would appear that Gimap5 in Rodentia has diverged in sequence from other taxa of the Mammalia lineage.

Gimap3 is anchored into the endoplasmic reticulum

The intracellular localization of tail-anchored Gimap family members has been controversial (Wong *et al.* 2010). The original localization study for Gimap3 demonstrated that the tail-anchor sequence of the protein was required for membrane insertion and was proposed to be the outer mitochondrial membrane (Daheron *et al.* 2001). Unfortunately closer examination of the data suggests that the findings could not properly distinguish between organelles. We decided to revisit the intracellular localization for Gimap3 in more detail.

The first test was to determine with which organelles endogenous Gimap3 would sediment on a Histodenz gradient. A postnuclear spleen lysate was separated in a stepwise

discontinuous Histodenz gradient to determine the sedimentation profile of Gimap3. Fractions were collected and used for immunoblotting using polyclonal antisera against Gimap3 (Figure S1). The sedimentation profile for endogenous Gimap3 was similar to the ER chaperone Calnexin but not to mitochondrial proteins in the outer mitochondrial membrane (Porin) and the matrix (Sdha) (Figure 2A).

Unfortunately, our polyclonal antibody against Gimap3 was ineffective for indirect immunofluorescence and thus unable to be used for determining intracellular localization by light microscopy. Therefore, we generated a chimeric Gimap3 with RFP fused at the N terminus of the protein to circumvent this problem (Figure 2B). This RFP construct should not affect the membrane targeting of the protein since tail-anchored proteins require only the C-terminal transmembrane domain and flanking residues for membrane insertion and retention (Rapaport 2003). Stable retroviral transduction or transient expression of this Gimap3 construct consistently localized to the ER and not mitochondria (Figure 2, C and D). Only the 39 amino acids at the C terminus were required for this ER localization (Figure 2, E and F). Furthermore, replacing the last 32 C-terminal amino acids with a tail-anchor sequence from Omp25, a *bona fide* outer mitochondrial membrane protein (Nemoto and De Camilli 1999) redirects Gimap3 to the outer mitochondrial membrane (Figure 2G). Collectively, these data suggest that Gimap3 localizes to the ER.

The expression level of Gimap3 modulates mtDNA segregation

To investigate how allelic expression of *Gimap3* modulates mtDNA segregation in the spleen, we first tested whether there were quantitative differences in the expression of these two murine alleles. The mRNA expression was quantified of both the CAST/Ei and BALB/c alleles in 3-month-old mice from an F2 (BALB/c × CAST/Ei) cross, which were heterozygous for these two *Gimap3* alleles. At 3 months of age most F2 mice display quantitative differences in the mtDNA segregation rate in hematopoietic tissues and are considered positive for segregation (Jokinen *et al.* 2010). However, there is also a subset of mice in this F2 cross that at 3 months of age can be identified while mtDNA segregation cannot yet be detected in hematopoietic tissues (Jokinen *et al.* 2010). These mice were considered negative for segregation. A semiquantitative RT–PCR approach was used to quantify the expression differences of these two alleles in the F2 mice utilizing a primer set that bind in exons 3 and 5 to amplify across exon 4, which is only 35 nucleotides long with a stretch of poly(A)'s and the only unique feature within the *Gimap3* mRNA to distinguish between the BALB/c and CAST/Ei alleles. The mRNA expression was quantified against a standard curve generated with equimolar ratios of BALB/c and CAST/Ei RNA. In mice positive for mtDNA selection there was a significantly stronger expression from the BALB *Gimap3* allele relative to the CAST *Gimap3* allele ($P < 0.001$) (Figure 3A).

Next, we investigated whether the difference in *Gimap3* mRNA expression resulted in a corresponding effect on the steady-state protein levels. Spleen homogenates were prepared from BALB/c, CAST/Ei, and F2 (BALB/c × CAST/Ei) mice heterozygous at the *Gimap3* locus for immunoblotting. Both Gimap3 protein variants can be expressed in cultured cells and detected by immunoblotting using our allele-specific polyclonal antibodies (Figure 3B and Figure S1). To our surprise there was no detectable Gimap3 protein (Figure 3B) in spleen lysates from CAST/Ei mice. This is in contrast to the abundant protein expression of the BALB/c Gimap3 (Figure 3B). In F2 (BALB/c × CAST/Ei) mice we also could not detect the CAST Gimap3 protein. Moreover, in these F2 mice the abundance of the BALB Gimap3 protein was reduced ~50% compared to spleens from BALB/c mice (Figure 3B), suggesting a dosage effect on the steady-state protein abundance of Gimap3.

To confirm the expression of the CAST/Ei *Gimap3* mRNA, we analyzed total spleen RNA by Northern blotting. Using three independent oligonucleotide probes that hybridize against sequences from exons 1–2, exon 3, and exons 4–5, we detected three transcripts (Figure 3C). All three probes were selected against sequence unique to *Gimap3* and not found in *Gimap5* (Figure 3C). As a positive control we used total RNA from murine embryonic fibroblasts ectopically expressing the BALB/c *Gimap3* cDNA consisting only of exons 4 and 5, which can be recognized only by probe c (Figure 3C). Probe c bound weakly to the CAST/Ei mRNA, which was not surprising, considering half of the probe recognizes nucleotides in exon 4, a region missing from the CAST/Ei mRNA. Assessing *Gimap3* expression using probe b, which hybridizes to exon 3, showed robust expression of both the BALB/c and CAST/Ei alleles in the spleen. These results confirm that although both Gimap3 alleles were expressed at the mRNA level, only the BALB/c variant could be detected in mouse spleens as a mature protein by immunoblotting.

The N terminus of CAST Gimap3 impairs protein synthesis

The inability to detect the CAST Gimap3 protein *in vivo* may be due to repressed synthesis of the polypeptide chain or in post-translational processing, such as cleavage of the N terminus and differential turnover. We pursued the hypothesis that protein synthesis of the CAST *Gimap3* was impaired because this allele has incorporated a uORF into the coding sequence for this protein. The presence of a uORF within a gene can act as a potent *in cis* post-transcriptional regulator of the main downstream ORF whereby protein synthesis of the uORF stalls ribosomes repressing translation of the downstream ORF (Morris and Geballe 2000; Calvo *et al.* 2009).

We wanted to first evaluate whether there was any difficulty in the synthesis of the uORF alone or fused to a nonnative protein such as YFP. We generated constructs comprising amino acids 1–68 of CAST Gimap3 alone or fused to YFP at the N terminus (Figure 4A). This stretch of

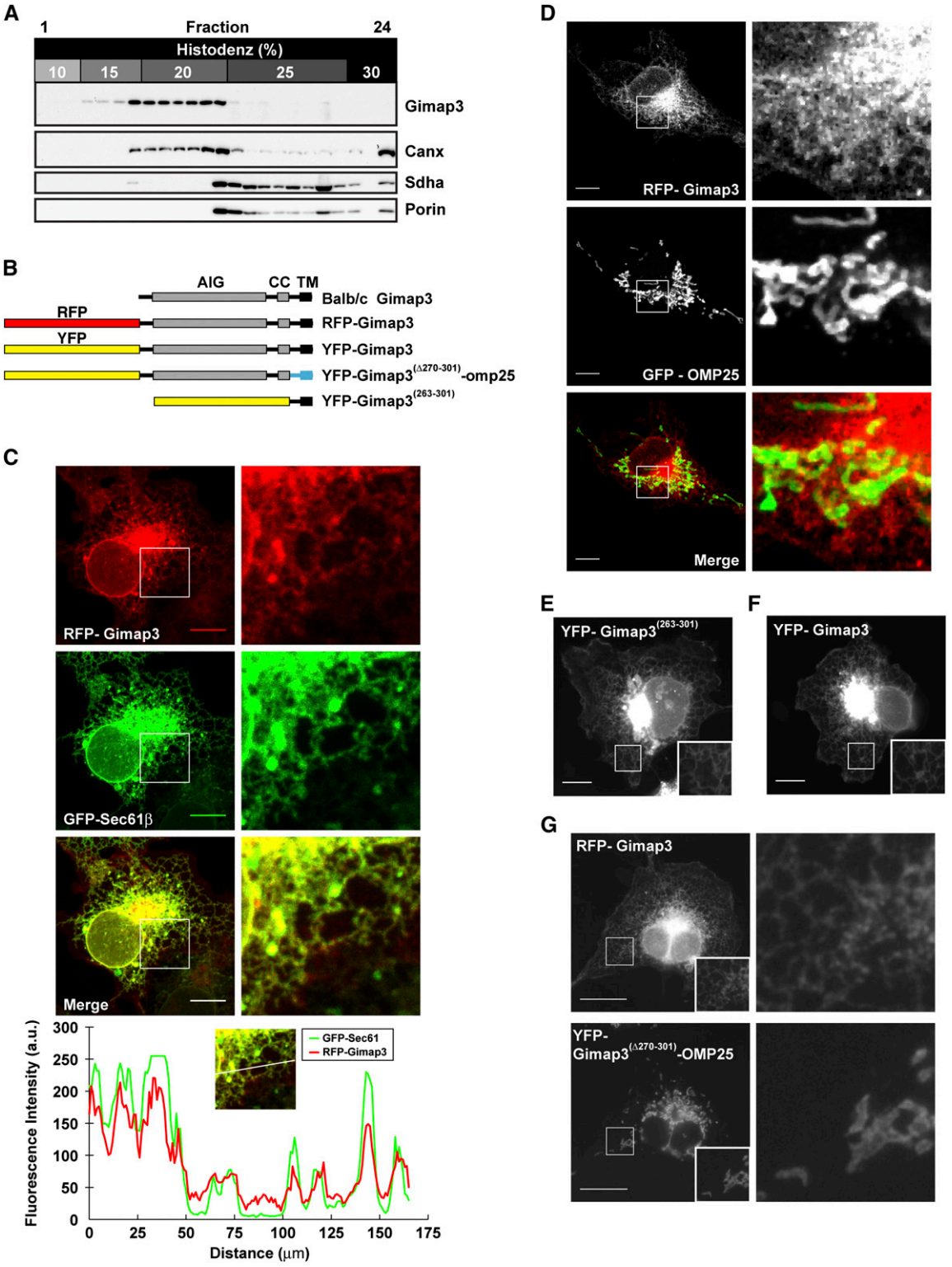

Figure 2 Gimap3 localizes to the endoplasmic reticulum. (A) Sedimentation profile of mouse postnuclear spleen lysate through a discontinuous Histodenz gradient. Fractions were separated by SDS–PAGE followed by immunoblotting with the indicated antibodies. Canx is an ER chaperone. Sdha and Porin are mitochondrial proteins localized in the matrix and outer membrane respectively. (B) A graphical illustration of the Gimap3 constructs used in microscopy. (C) Confocal images of COS-7 cells cotransfected with a chimeric RFP–Gimap3 and ER marker GFP–Sec61B. Below, line scans of the red and green channels. (D) Confocal images and inset magnifications of COS-7 cells cotransfected with the chimeric RFP–Gimap3 and the mitochondrial marker GFP–omp25. (E) COS-7 cells transfected with a construct containing only the C-terminal transmembrane domain of Gimap3 fused to YFP. (F) COS-7 cells transfected with a construct containing the full-length Gimap3 fused to the C terminus of YFP. (G) COS-7 cells cotransfected with RFP–Gimap3 and a chimeric YFP–Gimap3 missing the 32 C-terminal amino acids replaced with the omp25 sequence motif for mitochondrial localization. Scale bars, 10 μm.

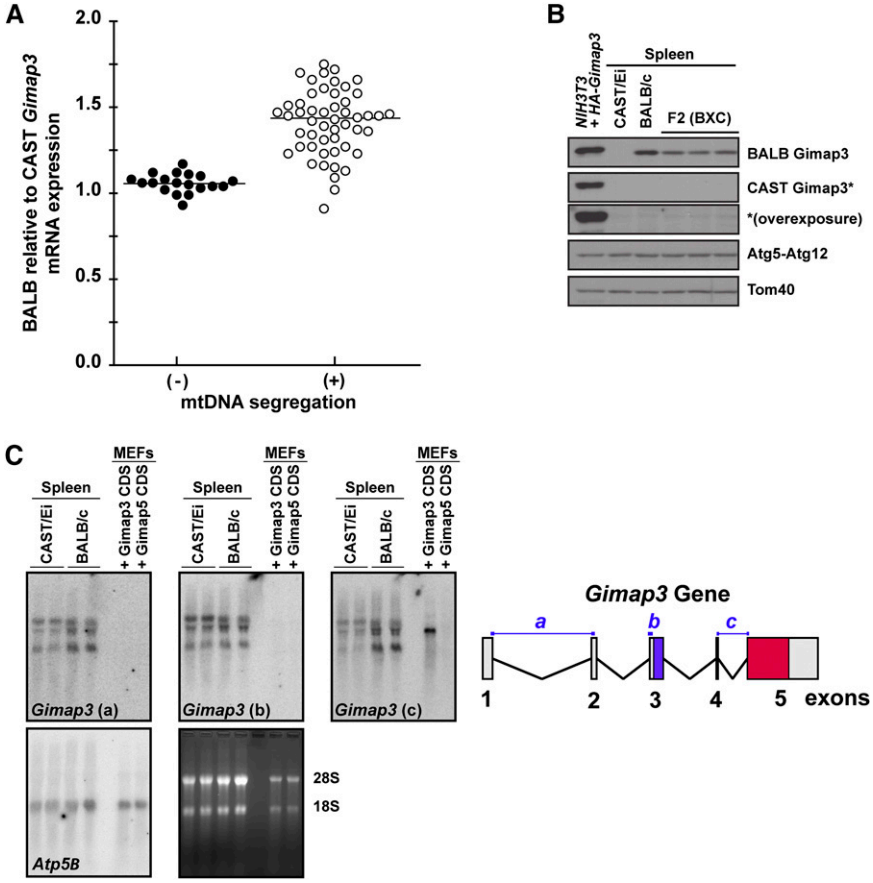

Figure 3 *Gimap3* expression affects mtDNA segregation in mouse spleen. (A) The expression level of the BALB/c *Gimap3* mRNA relative to CAST/Ei *Gimap3* by semiquantitative RT–PCR in F2 (BALB/c × CAST/Ei) mice heterozygous at the *Gimap3* locus. Mice were either positive (+) (n = 51) or negative (−) (n = 19) for mtDNA segregation. Mann–Whitney Test, $P < 0.001$. (B) Immunoblotting of total cell lysates from the spleen of BALB/c, CAST/Ei or F2 (BALB/c × CAST/Ei) mice. A NIH3T3 cell line was transduced with retroviruses expressing HA-tagged version of both the BALB/c *Gimap3* and CAST/Ei *Gimap3* was used as positive control. (*) Extended exposure with the CAST Gimap3 antibody. (C) Northern blot of total spleen RNA from CAST/Ei and BALB/c mice with three independent *Gimap3* probes (*a*–*c*) and a control probe for *Atp5B*. As positive and negative controls for the *Gimap3* probes total RNA was loaded from MEFs ectopically expressing the coding sequence (CDS) of BALB/c *Gimap3* and *Gimap5*. On the right, a graphical illustration of the *Gimap3* gene and location of the oligonucleotide probes.

polypeptides represents the only unique amino acids at the N terminus between the BALB and CAST Gimap3 (Jokinen *et al.* 2010). The objective was to express the constructs both *in vitro* and in cultured cells to test if there was difficulty in the synthesis of this polypeptide sequence and whether there was any post-translation regulation in the cell to modulate the steady-state protein abundance. We used a T7-promoter-coupled reticulocyte lysate assay with radiolabeled [^{35}S]methionine and cysteine to express these proteins *in vitro*. The linearity for the ^{35}S-radiolabel incorporation was established using YFP as a template cloned into the same vector backbone (Figure S2). Hereafter, the same conditions were used for expressing all constructs off the T7 promoter *in vitro*. Strikingly there was no detectable expression of the CAST$^{1–68}$ fragment alone (Figure 4B). Moreover, fusion of this CAST$^{1–68}$ fragment to YFP reduced the *in vitro* expression of the full-length protein compared to YFP (Figure 4, B and C). A prominent feature with the synthesis of CAST$^{1–68}$–YFP was consistent smearing of the mature protein (Figure 4B), which may be suggestive of stalled synthesis. In addition, there were smaller fragments generated with the CAST$^{1–68}$–YFP template, one of which comigrated with the full-length YFP (Figure 4B). Next we assessed the *in vitro* synthesis of full-length CAST *vs.* BALB Gimap3 (Figure 4, A and B). There was a reduction in the synthesis of the CAST Gimap3 compared to the BALB allele using the same T7-expression-coupled assay (Figure 4D). These data suggest that the N terminus of CAST Gimap3 exerts a negative effect on protein synthesis *in vitro*.

To evaluate the role of the uORF on protein synthesis in cultured cells we transiently transfected the plasmids into HEK293 cells followed by immunoblotting 24 hr post-transfection. For the CAST$^{1–68}$-YFP construct, most of the immunodetectable protein with an anti-GFP antibody comigrated through SDS–PAGE with full-length GFP and not near the expected molecular size of 35 kD as seen *in vitro* (Figure 4, B and E). Extended exposure with the anti-GFP antibody could detect a weaker band with the approximate size of the mature CAST$^{1–68}$–YFP (Figure 4E), showing that this protein can be synthesized *in vivo*. In contrast, using the CAST-specific polyclonal antibody we detected two prominent bands approximately of equal intensity for CAST$^{1–68}$–YFP that were more abundant than the steady-state level of full-length CAST Gimap3 (Figure 4F). There also was no detectable protein for the CAST$^{1–68}$, a finding consistent with the *in vitro* expression (Figure 4, B and F). Since the abundance of the full-length CAST–YFP differs between *in vitro* and *in vivo*, synthesis suggests that addtional factors are important for the steady-state level of the protein.

Stalled protein synthesis on ribosomes generates a stress to the cell, which typically activates mRNA surveillance pathways (Lykke-Andersen and Bennett 2014). As part of this stress response, polypeptide chains on stalled ribosomes are rapidly degraded by the proteasome (Lykke-Andersen

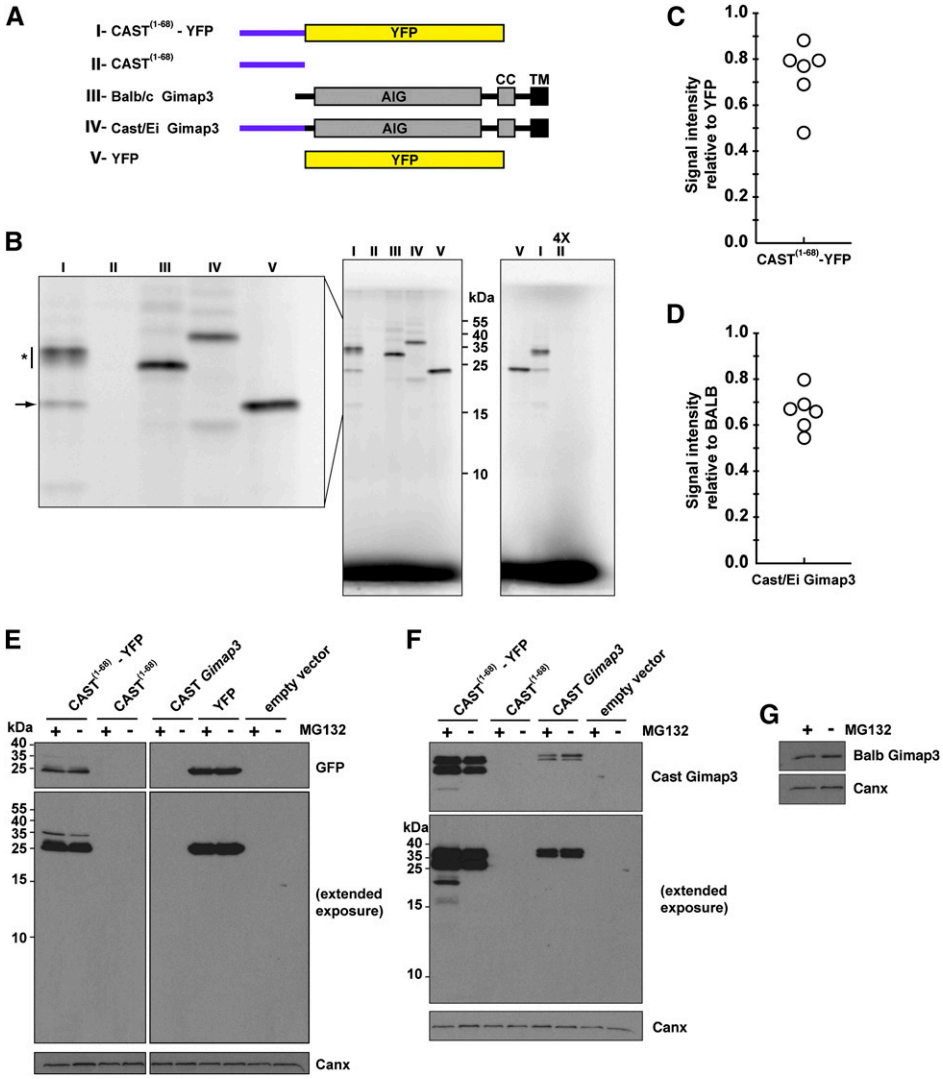

Figure 4 The N terminus of CAST Gimap3 impairs protein synthesis. (A) A graphical illustration of the Gimap3 constructs used. AIG, Gimap family domain; CC, coiled coil; TM, transmembrane domain. (B) SDS–PAGE of *in vitro* synthesis of proteins from a T7 promoter with [^{35}S]methionine and cysteine. Lanes numbered according to the constructs in A. (*) Consistent smearing of labeled protein. Arrow indicates labeled protein from CAST$^{(1–68)}$–YFP that comigrates with full-length YFP (lane V). Right: Four times excess sample was loaded for construct II. (C) Quantification of CAST$^{1–68}$–YFP *in vitro* production relative to YFP from six independent experiments. For the quantification, the smeared signal for CAST$^{(1–68)}$–YFP (* in B) was included along with the mature protein. (D) Quantification of CAST Gimap3 *in vitro* production relative to BALB Gimap3 from six independent experiments. (E and F) Immunoblotting of total cell lysates from HEK293 cells transfected with the indicated cDNA constructs and treated with the indicated antibodies. Cells were treated with or without MG132 7 hr prior to collection. (G) Immunoblotting of total cell lysates from HEK293 cells transfected with a *Gimap3* cDNA construct and treated with the indicated antibodies. Cells were treated with or without MG132 7 hr prior to collection.

and Bennett 2014) and thus stabilized only in the presence of proteasomal inhibitors, such as MG132. To test for evidence of the proteasome in modulating the abundance of the uORF we incubated cells with MG132. In cells expressing the CAST$^{1–68}$–YFP cDNA we observed smaller-molecular-weight fragments when treating with MG132 and using the CAST-specific antibody, but not the monoclonal anti-GFP antibody that detects only the mature protein (Figure 4, E and F). We also observed a shift with MG132 in the proportion of the two immunodetectable fragments expressed by CAST *Gimap3* (Figure 4F). In contrast, MG132 had no effect on the steady-state abundance of Gimap3 (Figure 4G). Since the CAST-specific antibody recognizes a stretch of 15 amino acid residues found only in the N terminus of the protein (Figure S1), the immunodetection of stable smaller-molecular-weight fragments when the proteasomal function is blocked may be attributable to the partial synthesis of the CAST$^{1–68}$–YFP because of ribosome stalling.

Next, we wanted to confirm this interpretation by testing whether the synthesis of CAST$^{1–68}$–YFP on polysomes was affected following the treatment of cells with MG132. Isokinetic sucrose density gradients were used to separate ribosomes and polysomes from treated cells (Figure 5). We found an increase in the CAST$^{1–68}$–YFP on polysomes following MG132 treatment (Figure 5) suggesting that the uORF fused to YFP leads to proteasomal turnover. Moreover, this analysis demonstrates that the predominant protein generated from the CAST$^{1–68}$–YFP cDNA comigrates with the molecular size of YFP when we used the anti-GFP antibody for immunoblotting (Figure 5, C and D). This is consistent with our previous findings (Figure 4E) and indicates the potential for ribosomes scanning through the uORF sequence to initiate translation on the AUG of YFP. Using the CAST antibody we also detected another truncated protein that was >25 kD (Figure 5D, bottom) and must contain an N terminus with the CAST polypeptide sequence. Collectively, these data suggest that the uORF in *Gimap3* mediates a negative effect on protein synthesis, possibly by stalling synthesis on ribosomes, and may account for the decreased abundance of CAST Gimap3 in mouse spleen.

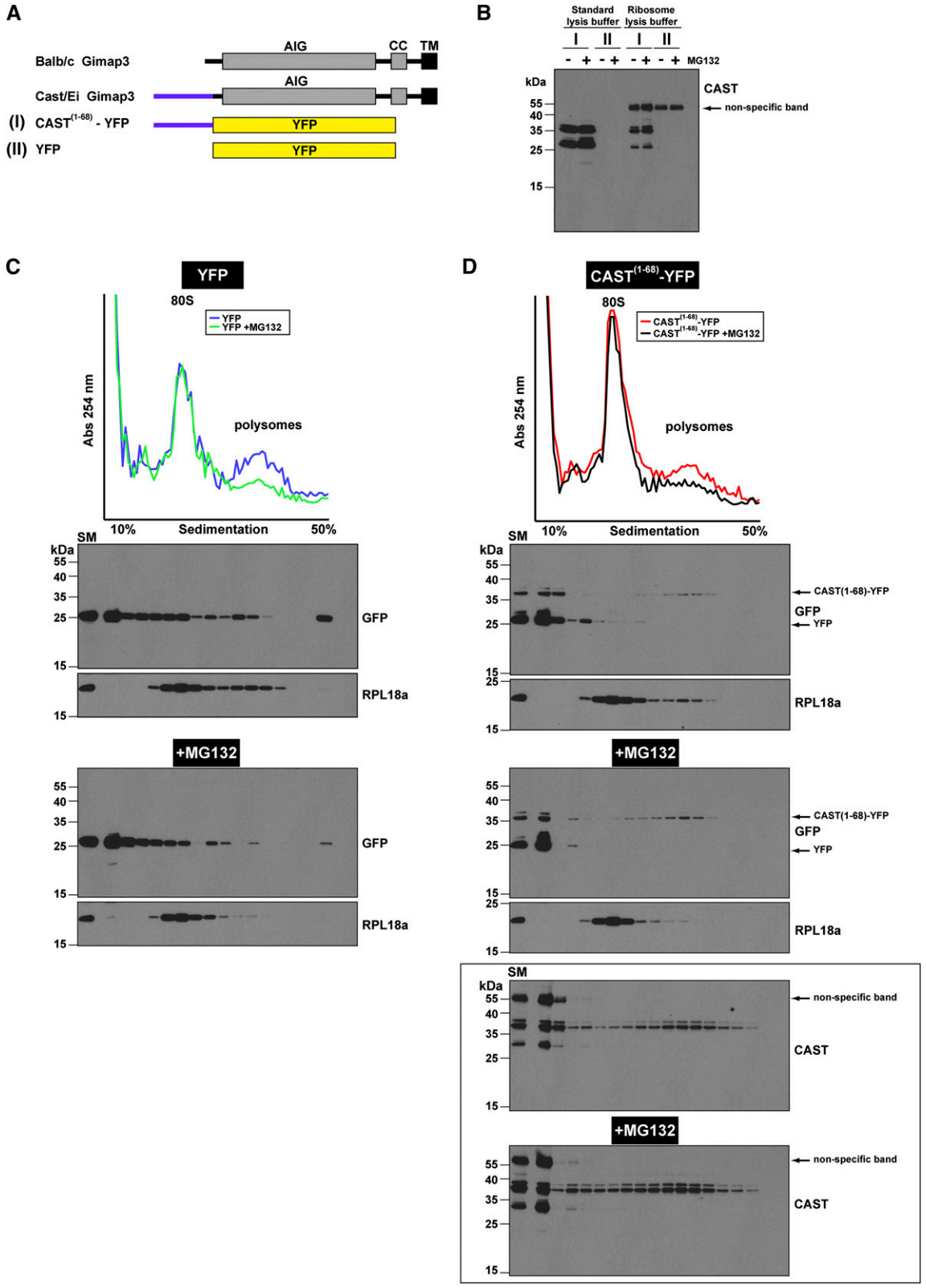

Figure 5 The CAST$^{(1–68)}$ polypeptide impairs protein synthesis and leads to accumulation on polysomes following proteasome inhibition. (A) A graphical illustration of the Gimap3 and YFP constructs. AIG, Gimap family domain; CC, coiled coil; TM, transmembrane domain. (B) Immunoblotting with the CAST polyclonal antibody comparing immunoreactivity of HEK293 lysates generated with different buffers and detergent combinations. The standard lysis buffer is used in Figure 4, whereas the ribosome lysis buffer is optimized for polysome profiles. (C and D) Polysome profiles of YFP and CAST$^{(1–68)}$–YFP. Total cell lysates from HEK293 cells transfected with the indicated cDNAs were prepared with the ribosome lysis buffer and separated on 10–50%

Gimap3 and Gimap5 are important for mtDNA segregation

Our original cloning of *Gimap3* as a modifier of mtDNA segregation (Jokinen *et al.* 2010) was unable to determine whether other *Gimap* family members, in particular the paralogue *Gimap5*, may also contribute to this mtDNA phenotype. Recent evidence points to a cooperative genetic function between *Gimap3* and *Gimap5* in lymphocyte development (Yano *et al.* 2014). To test *Gimap5* for a role in mtDNA segregation, we took advantage of a germline knockout mouse *Gimap5*^{tm1Wlr} (Schulteis *et al.* 2008). Homozygous *Gimap5*^{tm1Wlr} mice exhibit a severe hematopoietic stem cell defect, which leads to a reduced number of mature lymphocytes and lack of detectable NK cells (Schulteis *et al.* 2008). In *Gimap5*$^{tm1Wlr/WT}$ there are no reported defects in hematopoiesis or on the mRNA expression of other *Gimap* family members in the thymus; these mice were described only as having a 50% reduction in *Gimap5* expression (Schulteis *et al.* 2008). This dosage effect on *Gimap5* expression in heterozygotes has been consistently observed with two other independent murine *Gimap5* null mutations at both the mRNA and protein level in Barnes *et al.* (2010) and Yano *et al.* (2014), suggesting a tight correlation between *Gimap5* gene expression and protein abundance.

To test whether changes in the expression of *Gimap5* affect mtDNA segregation, we crossed our heteroplasmic mouse model (NZB and BALB mtDNA haplotypes) to *Gimap5*^{tm1Wlr}. Since both mouse lines were already established on the BALB/c nuclear background, no further backcrossing was required. In the spleen of homozygous *Gimap5*^{tm1Wlr} mice there are severe cellular and morphological abnormalities: a ninefold reduction in splenic T cells and a twofold reduction in total splenic cellularity (Schulteis *et al.* 2008). These pathological features in the spleens of *Gimap5*^{tm1Wlr} homozygote mice complicate the analysis of mtDNA segregation because the cellular composition of the organ is dramatically altered, which in turn affects *Gimap3* expression in this tissue (Figure 6A and Figure S3). Therefore, we focused our mtDNA segregation analysis on *Gimap5*$^{tm1Wlr/WT}$ because these mice are phenotypically indistinguishable from wild type and display no signs of pathology or cellularity defects in the spleen, but have a 50% decrease in Gimap5 abundance.

In the hematopoietic compartment of wild-type heteroplasmic mice mtDNA segregation can be modeled as an exponential decay, so that by 100 days of post-natal life there is an ~50% decrease in the proportion of NZB mtDNA in leukocytes of both myeloid and lymphoid lineages (Battersby *et al.* 2005). We found a significant difference in mtDNA segregation of *Gimap5*$^{tm1Wlr/WT}$ in both the spleen and bone marrow compared to wild-type littermate controls (Figure 6B). The effect is more modest in the spleen compared to the bone marrow (Figure 6B) because within the spleen the supporting stromal cells are neutral with respect to mtDNA segregation (Battersby *et al.* 2005).

Since we found that changes in Gimap3 abundance were accompanied with an effect on mtDNA segregation, we wanted to test whether in *Gimap5*$^{tm1Wlr/WT}$ there was any effect on the abundance of Gimap3. Total cell lysates were prepared from isolated splenocytes for immunoblotting demonstrating a 50% reduction in Gimap3 protein abundance compared to wild type (Figure 6C) even though there was no difference in the expression of the *Gimap3* mRNA (Figure 6A). These findings provide further support for a cooperative function between Gimap3 and Gimap5 and indicate that the steady-state abundance of these two proteins is an important factor for the segregation of mtDNA haplotypes in mouse leukocytes.

A 50% reduction of Gimap3 and Gimap5 protein levels was sufficient to significantly modulate mtDNA segregation in leukocytes and suggests that the identification of other factors dependent upon *Gimap5* may provide insight into the molecular connection to the segregation of the mitochondrial genome. To identify such factors we used a quantitative proteomic approach with iTRAQ (isobaric tags for relative and absolute quantification) labeling followed by LC-MS/MS analysis of postnuclear membrane enrichments generated from spleens of wild type and *Gimap5*^{tm1Wlr} heterozygote littermates (File S1 and File S2)(Lietzen *et al.* 2011). Three independent biological replicates for each genotype were used for the iTRAQ analysis, which led to the identification of >1100 distinct proteins (File S1). We were unable to quantify Gimap3 and Gimap5 using this approach with any confidence because the sequence homology between these two proteins is very high (84% identity) and the number of unique peptide sequences detected by LC-MS/MS was inadequate for confident identification and iTRAQ quantification. In *Gimap5*$^{tm1Wlr/WT}$ we detected robust changes in the abundance of five proteins that all have a connection to the regulation of the cytoskeleton and cell motility via small GTPase signaling (Table1). The abundance of these proteins was also further affected in *Gimap5*^{tm1Wlr} homozygotes (File S2). Since Gimap5 is a membrane-anchored lysosomal protein, this points to a quantitative effect of *Gimap5* expression on the interaction between organelles and the cytoskeleton during cell motility as an important factor in mtDNA segregation of hematopoietic cell lineages in mice.

Discussion

The mechanisms governing the segregation of mitochondrial genomes are still poorly understood despite considerable efforts since the discovery of pathogenic mtDNA mutations (Jokinen and Battersby 2013). We followed up our cloning of *Gimap3* as a modifier of mtDNA segregation in mice to determine how allelic variants of this gene influence the phenotype. The most important finding from this study is

sucrose gradients. SM, starting material. Top: Absorbance at 254 nm of 82 fractions collected from the top. Below, immunoblotting of TCA precipitated fractions from five pooled aliquots from the top with the indicated antibodies and with equal film exposures ±MG132

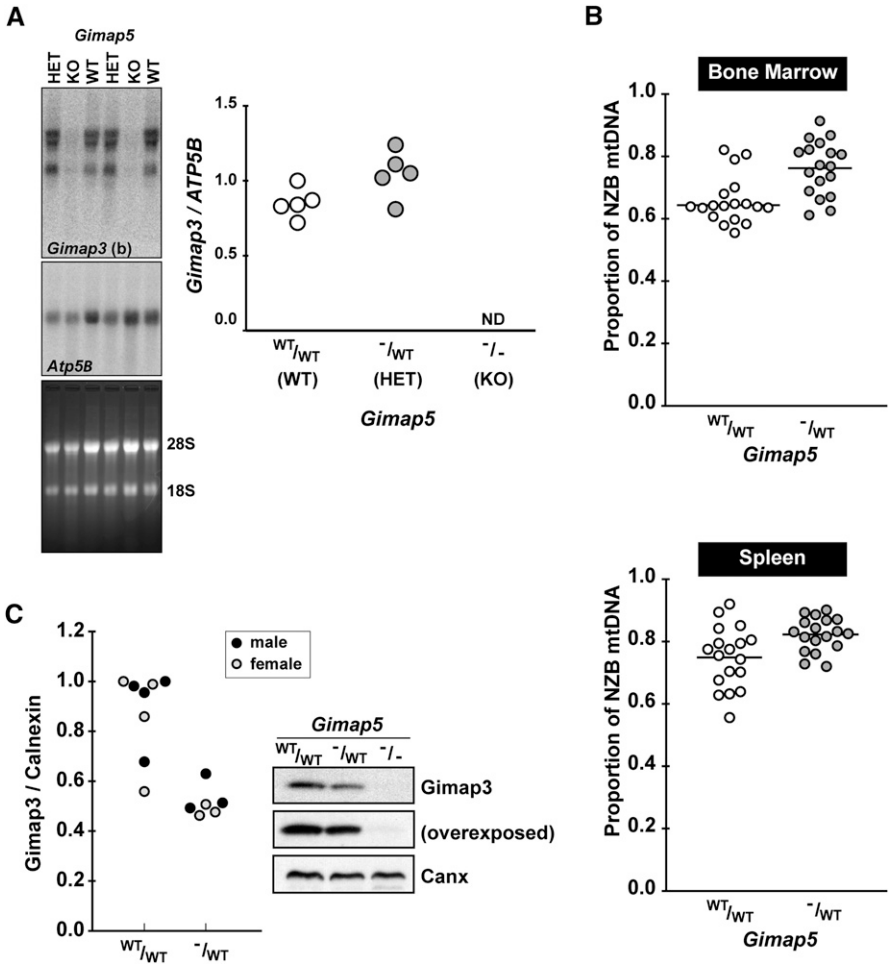

Figure 6 Genetic loss of *Gimap5* affects Gimap3 and mtDNA segregation. (A) Northern blot of spleen total RNA from wild-type *Gimap5*, *Gimap5*$^{tm1Wlr/WT}$, and homozygote *Gimap5*^{tm1Wlr} mice hybridized with *Gimap3* (*b*) probe and control probe *Atp5B*. Right: Quantification of *Gimap3* mRNA compared to *Atp5B*. (B) Decreased selection against the NZB mtDNA genome in the bone marrow and spleen of *Gimap5*$^{tm1Wlr/WT}$ compared to wild-type littermate controls. $n = 18$ for each group; (*) $P < 0.01$ two-tailed *t*-test; means are indicated by the line through the scatter plot. Mice were 70 days of postnatal age at the time of sampling. (C) A representative immunoblotting of Gimap3 from whole-cell lysates from isolated splenocytes of wild type, *Gimap5*$^{tm1Wlr/WT}$ and homozygote *Gimap5*^{tm1Wlr} mice. Left: Quantification of Gimap3 abundance compared to Calnexin.

that expression differences in *Gimap3* and *Gimap5* appear to be a critical factor to the segregation of the mitochondrial genome in mouse hematopoietic tissues.

Regulation of *Gimap3* expression is complex and possibly involves cell-specific modulators. The incorporation of a uORF into the coding sequence of the *M. m. castaneus Gimap3* has a negative effect on protein synthesis potentially through translation repression. Our data are consistent with a variable penetrance of the uORF on the CAST Gimap3, as the expression and stability of the mature protein decreases steadily from *in vitro* synthesis to ectopic expression in nonhematopoietic cell types to the undetectable levels *in vivo* in mouse leukocytes. This is in contrast to the BALB Gimap3 that can be robustly detected in the mouse. Since our polyclonal antibodies do not recognize both protein alleles, we cannot exclude the possibility of N-terminal processing of CAST Gimap3 in mice. UORFs have been described as translation regulatory sequences and are estimated to be present in >40% of human and mouse transcripts (Calvo *et al.* 2009). The mechanism of action for uORFs often involves repressing translation of the downstream (main) open reading frame (Morris and Geballe 2000; Calvo *et al.* 2009). Such a regulatory mechanism allows for rapid changes in the protein abundance upon stress conditions, when *trans* factors can release the uORF repression of translation (Barbosa *et al.* 2013). Our data also indicate that ribosomes may scan through this uORF sequence and initiate translation on a downstream AUG even though there is stronger sequence conservation to the Kozak consensus in the uORF. Further work is required to elucidate the regulatory role of the uORF on the expression of *Gimap3* alleles in mice.

We show that Gimap3 localizes to the ER and not mitochondria as previously reported. How then could a resident protein of the ER affect mtDNA segregation? Interactions between the ER and mitochondria play a key role in many aspects of mitochondrial homeostasis, such as morphology of the mitochondrial reticulum (division and tethering of the organelle), calcium handling, lipid transfer, and transmission of the mitochondrial genome among others (de Brito and Scorrano 2008; Kornmann *et al.* 2009; Friedman *et al.* 2011; Hoppins *et al.* 2011; Connerth *et al.* 2012; Rowland and Voeltz 2012; Korobova *et al.* 2013; Hajnoczky *et al.* 2014). Any number of these functions could be important to mtDNA segregation.

Why the need to restrict the expression of these Gimap protein scaffolds to the hematopoietic compartment? Leukocytes have a relatively small cytosolic volume with few organelles by comparison to most cell types and are one of the most dynamic cell types in mammals as they migrate

Table 1 Proteins whose abundance in mouse splenocytes is dependent upon *Gimap5*: iTRAQ analysis comparing *Gimap5*$^{WT/WT}$ to *Gimap5*$^{tm1Wlr/WT}$ littermates

Protein	Fold change het/wt	Biological process
Cyfip2	0.55	Component of WAVE complex for assembly of F-actin complex
Arhgdia	0.57	Rho protein signal transduction, regulation of protein localization
Vasp	0.57	Actin cytoskeleton reorganization
Elmo1	1.83	Actin filament-based process, phagocytosis
S100A9	2.12	Actin cytoskeleton reorganization, leukocyte chemotaxis, phagocytosis

throughout the body by chemotaxis. Chemotaxis and receptor signaling at the immunological synapse both require dynamic and coordinated reorganization of organelle distribution, especially mitochondria (Campello *et al.* 2006; Quintana *et al.* 2007). During chemotaxis, leukocytes become polarized with mitochondria relocalized to the uropod. Disrupting this mitochondrial relocalization impairs the ability of a leukocyte to migrate (Campello *et al.* 2006; Quintana *et al.* 2007). Recent reports from mammalian systems suggest that interactions with the actin cytoskeleton are needed for mitochondrial division (Korobova *et al.* 2013) and dynamics during formation of the immunological synapse (Schwindling *et al.* 2010). The stoichiometric changes in *Gimap5*^{tm1Wlr} heterozygotes of factors interacting with the actin cytoskeleton could suggest that these Gimap scaffolds are important for the dynamic organization and coordination of organelle movement during chemotaxis. Consistent with this interpretation is the recent work on Gimap4 showing that this soluble member of the Gimap family mediates an interaction between the *trans* Golgi network and the actin cytoskeleton to sustain for interferon gamma secretion (Heinonen *et al.* 2014). Since Gimap3 and Gimap5 reside in the membrane of different organelles, it is tempting to hypothesize that these proteins could help mediate organelle distribution, organization, and contact within the cell, which in turn would affect segregation of the mitochondrial genome in leukocyte lineages.

The absence of *Gimap3* in most current mammalian genome annotations could indicate that the gene function has been lost or taken over by *Gimap5*, or could be due to poor resolution of current genome annotations because of the high sequence similarity between *Gimap3* and *Gimap5*. Therefore the overall importance of *Gimap3* across mammals, let alone vertebrates, is at present difficult to conclude, as it might be restricted to mice. However, analysis of the C-terminal protein sequence of Gimap5 across mammalian taxa suggests the evolution of *Gimap5* in Rodentia differs considerably from other mammalian clades. Clearly, further research is required to resolve this issue.

The regulation of mtDNA segregation in metazoans remains a complex genetic problem. In the majority of cases, selection for specific mtDNA haplotypes in mammals is not based upon detectable differences in mitochondrial oxidative phosphorylation or on the replication rate of the genome (Jokinen and Battersby 2013). Thus, in mammals the identity of regulatory mechanisms that coordinate the segregation of the mitochondrial genome remain intractable despite considerable effort by the field (Jokinen and Battersby 2013). The forward genetic approaches we have taken have provided a degree of insight into the nuclear control of mtDNA segregation. Nonetheless, progress remains slow as the problem can be investigated only in mice because cultured cells cannot faithfully replicate the mtDNA segregation patterns observed in mammals (Jokinen and Battersby 2013). In the end, selection for a particular mtDNA haplotype within a specific tissue can occur only at three levels: the cell, organelle, or genome. Two fundamental components are required for such a mechanism to work: signal generation that distinguishes mtDNA variants or mutations and the molecular machinery to act on or interpret those signals. Such a signal can be generated only at the sequence level, nucleic acid and or polypeptide, or by the functional consequences derived from those sequences. There appears to be tissue-specific differences in either the generation or interpretation of these signals in our mouse model. Based upon our findings, the segregation of mtDNA haplotypes in the mouse hematopoietic compartment may be dependent upon the regulation of an intrinsic property of these cell types to coordinate organelle interactions as they migrate throughout the body.

Acknowledgments

We thank Uwe Richter, Anu Wartiovaara, and Howy Jacobs for discussion. We thank the Biomedicum Imaging Unit (BIU) for the confocal facilities. The Academy of Finland Center of Excellence—FinMIT, the University of Helsinki, and the Jane and Aatos Erkko Foundation support research in the BJB laboratory. R.J. was supported by Helsinki Biomedical Graduate Program, Emil Aaltonen Foundation, Biomedicum-Helsinki Foundation, the Waldemar von Frenckell Foundation, and the Finnish Cultural Foundation. H.W. was supported by National Institute of Allergy and Infectious Diseases AI42380. T.A.N.'s laboratory is supported by the Academy of Finland (135628 and 140950) and the University of Helsinki. A.J.K. and J.K.H. were supported by grants from the Academy of Finland and the Sigrid Juselius Foundation. The authors declare no conflict of interest.

Literature Cited

Barbosa, C., I. Peixeiro, and L. Romao, 2013 Gene expression regulation by upstream open reading frames and human disease. PLoS Genet. 9: e1003529.

Barnes, M. J., H. Aksoylar, P. Krebs, T. Bourdeau, C. N. Arnold *et al.*, 2010 Loss of T cell and B cell quiescence precedes the onset of

microbial flora-dependent wasting disease and intestinal inflammation in Gimap5-deficient mice. J. Immunol. 184: 3743–3754.
Battersby, B. J., and E. A. Shoubridge, 2001 Selection of a mtDNA sequence variant in hepatocytes of heteroplasmic mice is not due to differences in respiratory chain function or efficiency of replication. Hum. Mol. Genet. 10: 2469–2479.
Battersby, B. J., J. C. Loredo-Osti, and E. A. Shoubridge, 2003 Nuclear genetic control of mitochondrial DNA segregation. Nat. Genet. 33: 183–186.
Battersby, B. J., M. E. Redpath, and E. A. Shoubridge, 2005 Mitochondrial DNA segregation in hematopoietic lineages does not depend on MHC presentation of mitochondrially encoded peptides. Hum. Mol. Genet. 14: 2587–2594.
Boulet, L., G. Karpati, and E. A. Shoubridge, 1992 Distribution and threshold expression of the tRNA(Lys) mutation in skeletal muscle of patients with myoclonic epilepsy and ragged-red fibers (MERRF). Am. J. Hum. Genet. 51: 1187–1200.
Burgstaller, J. P., I. G. Johnston, N. S. Jones, J. Albrechtova, T. Kolbe *et al.*, 2014 MtDNA segregation in heteroplasmic tissues is common in vivo and modulated by haplotype differences and developmental stage. Cell Rep. 7: 2031–2041.
Calvo, S. E., D. J. Pagliarini, and V. K. Mootha, 2009 Upstream open reading frames cause widespread reduction of protein expression and are polymorphic among humans. Proc. Natl. Acad. Sci. USA 106: 7507–7512.
Campello, S., R. A. Lacalle, M. Bettella, S. Manes, L. Scorrano *et al.*, 2006 Orchestration of lymphocyte chemotaxis by mitochondrial dynamics. J. Exp. Med. 203: 2879–2886.
Chen, Y., M. Yu, X. Dai, M. Zogg, R. Wen *et al.*, 2011 Critical role for Gimap5 in the survival of mouse hematopoietic stem and progenitor cells. J. Exp. Med. 208: 923–935.
Chinnery, P. F., and D. C. Samuels, 1999 Relaxed replication of mtDNA: a model with implications for the expression of disease. Am. J. Hum. Genet. 64: 1158–1165.
Chinnery, P. F., N. Howell, R. N. Lightowlers, and D. M. Turnbull, 1997 Molecular pathology of MELAS and MERRF: the relationship between mutation load and clinical phenotypes. Brain 120(10): 1713–1721.
Chinnery, P. F., P. J. Zwijnenburg, M. Walker, N. Howell, R. W. Taylor *et al.*, 1999 Nonrandom tissue distribution of mutant mtDNA. Am. J. Med. Genet. 85: 498–501.
Connerth, M., T. Tatsuta, M. Haag, T. Klecker, B. Westermann *et al.*, 2012 Intramitochondrial transport of phosphatidic acid in yeast by a lipid transfer protein. Science 338: 815–818.
Daheron, L., T. Zenz, L. D. Siracusa, C. Brenner, and B. Calabretta, 2001 Molecular cloning of Ian4: a BCR/ABL-induced gene that encodes an outer membrane mitochondrial protein with GTP-binding activity. Nucleic Acids Res. 29: 1308–1316.
de Brito, O. M., and L. Scorrano, 2008 Mitofusin 2 tethers endoplasmic reticulum to mitochondria. Nature 456: 605–610.
Dunbar, D. R., P. A. Moonie, H. T. Jacobs, and I. J. Holt, 1995 Different cellular backgrounds confer a marked advantage to either mutant or wild-type mitochondrial genomes. Proc. Natl. Acad. Sci. USA 92: 6562–6566.
Elias, J. E., and S. P. Gygi, 2007 Target-decoy search strategy for increased confidence in large-scale protein identifications by mass spectrometry. Nat. Methods 4: 207–214.
Friedman, J. R., L. L. Lackner, M. West, J. R. DiBenedetto, J. Nunnari *et al.*, 2011 ER tubules mark sites of mitochondrial division. Science 334: 358–362.
Fu, K., R. Hartlen, T. Johns, A. Genge, G. Karpati *et al.*, 1996 A novel heteroplasmic tRNAleu(CUN) mtDNA point mutation in a sporadic patient with mitochondrial encephalomyopathy segregates rapidly in skeletal muscle and suggests an approach to therapy. Hum. Mol. Genet. 5: 1835–1840.
Hagstrom, E., C. Freyer, B. J. Battersby, J. B. Stewart, and N. G. Larsson, 2014 No recombination of mtDNA after heteroplasmy for 50 generations in the mouse maternal germline. Nucleic Acids Res. 42: 1111–1116.
Hajnoczky, G., D. Booth, G. Csordas, V. Debattisti, T. Golenar *et al.*, 2014 Reliance of ER-mitochondrial calcium signaling on mitochondrial EF-hand Ca binding proteins: miros, MICUs, LETM1 and solute carriers. Curr. Opin. Cell Biol. 29C: 133–141.
Heinonen, M. T., K. Kanduri, H. J. Lahdesmaki, R. Lahesmaa, and T. A. Henttinen, 2015 Tubulin- and actin-associating GIMAP4 is required for IFN-gamma secretion during Th cell differentiation. Immunol. Cell Biol. 93: 158–166.
Hoppins, S., S. R. Collins, A. Cassidy-Stone, E. Hummel, R. M. Devay *et al.*, 2011 A mitochondrial-focused genetic interaction map reveals a scaffold-like complex required for inner membrane organization in mitochondria. J. Cell Biol. 195: 323–340.
Hornum, L., J. Romer, and H. Markholst, 2002 The diabetes-prone BB rat carries a frameshift mutation in Ian4, a positional candidate of Iddm1. Diabetes 51: 1972–1979.
Jenuth, J. P., A. C. Peterson, K. Fu, and E. A. Shoubridge, 1996 Random genetic drift in the female germline explains the rapid segregation of mammalian mitochondrial DNA. Nat. Genet. 14: 146–151.
Jenuth, J. P., A. C. Peterson, and E. A. Shoubridge, 1997 Tissue-specific selection for different mtDNA genotypes in heteroplasmic mice. Nat. Genet. 16: 93–95.
Jokinen, R., and B. J. Battersby, 2013 Insight into mammalian mitochondrial DNA segregation. Ann. Med. 45: 149–155.
Jokinen, R., P. Marttinen, H. K. Sandell, T. Manninen, H. Teerenhovi *et al.*, 2010 Gimap3 regulates tissue-specific mitochondrial DNA segregation. PLoS Genet. 6: e1001161.
Kawakami, Y., R. Sakuta, K. Hashimoto, O. Fujino, T. Fujita *et al.*, 1994 Mitochondrial myopathy with progressive decrease in mitochondrial tRNA(Leu)(UUR) mutant genomes. Ann. Neurol. 35: 370–373.
Kornmann, B., E. Currie, S. R. Collins, M. Schuldiner, J. Nunnari *et al.*, 2009 An ER-mitochondria tethering complex revealed by a synthetic biology screen. Science 325: 477–481.
Korobova, F., V. Ramabhadran, and H. N. Higgs, 2013 An actin-dependent step in mitochondrial fission mediated by the ER-associated formin INF2. Science 339: 464–467.
Krucken, J., R. M. Schroetel, I. U. Muller, N. Saidani, P. Marinovski *et al.*, 2004 Comparative analysis of the human gimap gene cluster encoding a novel GTPase family. Gene 341: 291–304.
Larsson, N. G., E. Holme, B. Kristiansson, A. Oldfors, and M. Tulinius, 1990 Progressive increase of the mutated mitochondrial DNA fraction in Kearns–Sayre syndrome. Pediatr. Res. 28: 131–136.
Lietzen, N., T. Ohman, J. Rintahaka, I. Julkunen, T. Aittokallio *et al.*, 2011 Quantitative subcellular proteome and secretome profiling of influenza A virus-infected human primary macrophages. PLoS Pathog. 7: e1001340.
Lykke-Andersen, J., and E. J. Bennett, 2014 Protecting the proteome: Eukaryotic cotranslational quality control pathways. J. Cell Biol. 204: 467–476.
MacMurray, A. J., D. H. Moralejo, A. E. Kwitek, E. A. Rutledge, B. Van Yserloo *et al.*, 2002 Lymphopenia in the BB rat model of type 1 diabetes is due to a mutation in a novel immune-associated nucleotide (Ian)-related gene. Genome Res. 12: 1029–1039.
Morris, D. R., and A. P. Geballe, 2000 Upstream open reading frames as regulators of mRNA translation. Mol. Cell. Biol. 20: 8635–8642.
Nemoto, Y., and P. De Camilli, 1999 Recruitment of an alternatively spliced form of synaptojanin 2 to mitochondria by the interaction with the PDZ domain of a mitochondrial outer membrane protein. EMBO J. 18: 2991–3006.
Nitta, T., and Y. Takahama, 2007 The lymphocyte guard-IANs: regulation of lymphocyte survival by IAN/GIMAP family proteins. Trends Immunol. 28: 58–65.

Nitta, T., M. Nasreen, T. Seike, A. Goji, I. Ohigashi *et al.*, 2006 IAN family critically regulates survival and development of T lymphocytes. PLoS Biol. 4: e103.

Okado-Matsumoto, A., and I. Fridovich, 2001 Subcellular distribution of superoxide dismutases (SOD) in rat liver: Cu,Zn-SOD in mitochondria. J. Biol. Chem. 276: 38388–38393.

Quintana, A., C. Schwindling, A. S. Wenning, U. Becherer, J. Rettig *et al.*, 2007 T cell activation requires mitochondrial translocation to the immunological synapse. Proc. Natl. Acad. Sci. USA 104: 14418–14423.

Rapaport, D., 2003 Finding the right organelle: targeting signals in mitochondrial outer-membrane proteins. EMBO Rep. 4: 948–952.

Rowland, A. A., and G. K. Voeltz, 2012 Endoplasmic reticulum-mitochondria contacts: function of the junction. Nat. Rev. Mol. Cell Biol. 13: 607–625.

Schulteis, R. D., H. Chu, X. Dai, Y. Chen, B. Edwards *et al.*, 2008 Impaired survival of peripheral T cells, disrupted NK/NKT cell development, and liver failure in mice lacking Gimap5. Blood 112: 4905–4914.

Schwefel, D., C. Frohlich, J. Eichhorst, B. Wiesner, J. Behlke *et al.*, 2010 Structural basis of oligomerization in septin-like GTPase of immunity-associated protein 2 (GIMAP2). Proc. Natl. Acad. Sci. USA 107: 20299–20304.

Schwefel, D., B. S. Arasu, S. F. Marino, B. Lamprecht, K. Kochert *et al.*, 2013 Structural insights into the mechanism of GTPase activation in the GIMAP family. Structure 21: 550–559.

Schwindling, C., A. Quintana, E. Krause, and M. Hoth, 2010 Mitochondria positioning controls local calcium influx in T cells. J. Immunol. 184: 184–190.

Shilov, I. V., S. L. Seymour, A. A. Patel, A. Loboda, W. H. Tang *et al.*, 2007 The Paragon Algorithm, a next generation search engine that uses sequence temperature values and feature probabilities to identify peptides from tandem mass spectra. Mol. Cell. Proteomics 6: 1638–1655.

Wai, T., D. Teoli, and E. A. Shoubridge, 2008 The mitochondrial DNA genetic bottleneck results from replication of a subpopulation of genomes. Nat. Genet. 40: 1484–1488.

Weber, K., J. N. Wilson, L. Taylor, E. Brierley, M. A. Johnson *et al.*, 1997 A new mtDNA mutation showing accumulation with time and restriction to skeletal muscle. Am. J. Hum. Genet. 60: 373–380.

Wong, V.W.Y., A. E. Saunders, A. Hutchings, J. C. Pascall, C. Carter *et al.*, 2010 The autoimmunity-related GIMAP5 GTPase is a lysosome-associated protein. Self Nonself 1: 259–268.

Yano, K., C. Carter, N. Yoshida, T. Abe, A. Yamada *et al.*, 2014 Gimap3 and Gimap5 cooperate to maintain T-cell numbers in the mouse. Eur. J. Immunol. 44: 561–572.

Communicating editor: J. C. Schimenti

GENETICS

Supporting Information
http://www.genetics.org/lookup/suppl/doi:10.1534/genetics.115.175596/-/DC1

Quantitative Changes in *Gimap3* and *Gimap5* Expression Modify Mitochondrial DNA Segregation in Mice

Riikka Jokinen, Taina Lahtinen, Paula Marttinen, Maarit Myöhänen, Pilvi Ruotsalainen, Nicolas Yeung, Antonina Shvetsova, Alexander J. Kastaniotis, J. Kalervo Hiltunen, Tiina Öhman, Tuula A. Nyman, Hartmut Weiler, and Brendan J. Battersby

Copyright © 2015 by the Genetics Society of America
DOI: 10.1534/genetics.115.175596

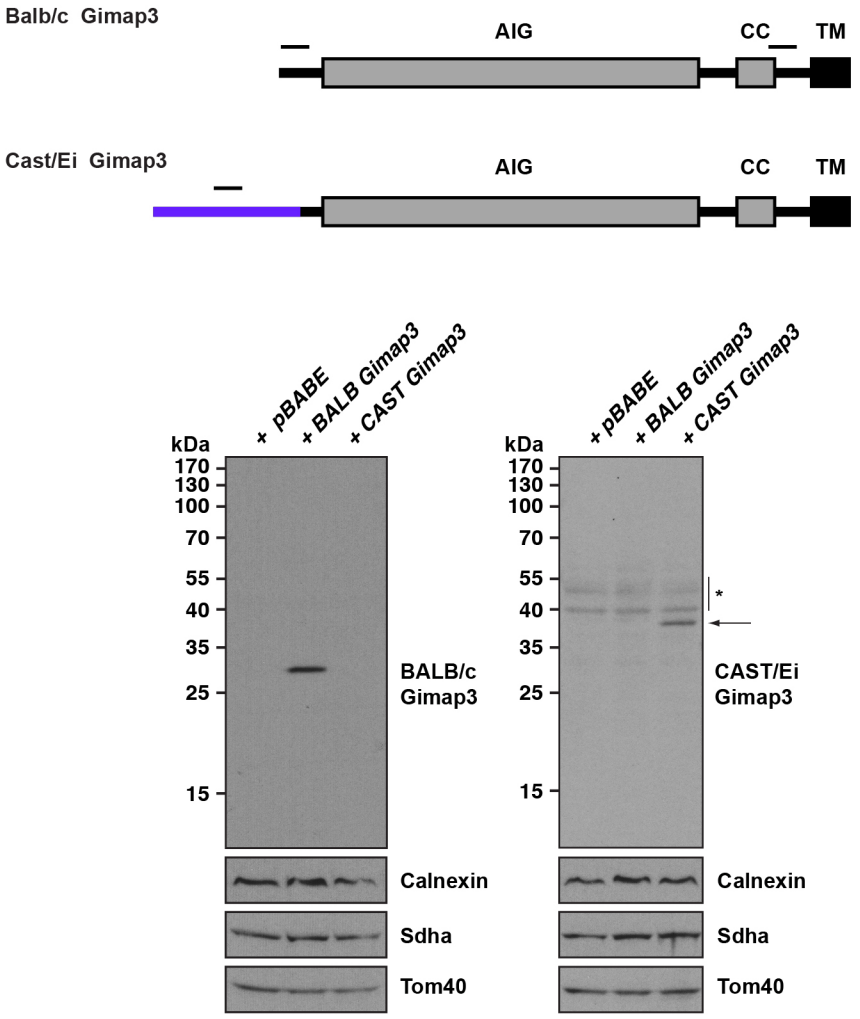

Figure S1: Validation of Gimap3 allele-specific polyclonal antibodies.
Upper panel, a graphical illustration of the Gimap3 protein for the BALB/c and CAST/Ei allelic variants. Black lines above the protein represent location of peptide sequences used for generating polyclonal antibodies. CC = coiled-coil; TM = transmembrane domain. Blue in the CAST/Ei protein indicates unique polypeptide sequence compared to the BALB/c allele. Lower panel, immunoblotting of whole cell lysates from retrovirally transduced mouse embryonic fibroblasts with the indicated cDNAs and antibodies.
* non-specific signal detected in mouse embryonic fibroblasts.

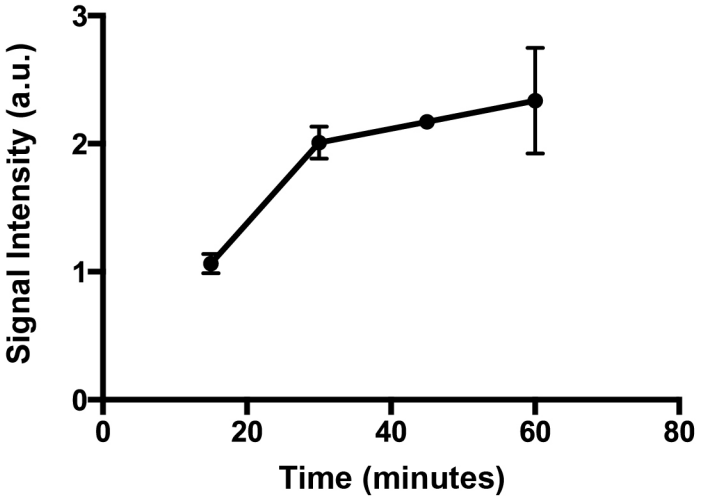

Figure S2: Quantification of ^{35}S-Met, Cys *in vitro* incorporation into YFP. YFP was produced in a coupled T7 reticulocyte lysate *in vitro* expression assay then separated by SDS-PAGE. The gel was dried, incubated with a phospho screen and signal intensity quantified following scanning with a Typhoon imaging station. Each time point represents a mean (+/- S.D.) of three independent experiments.

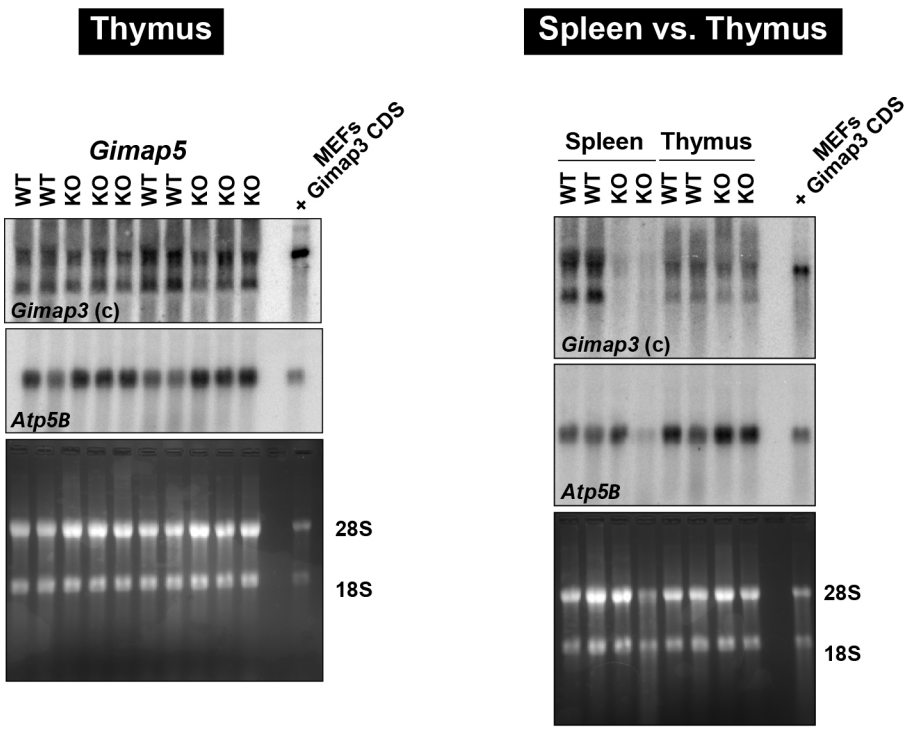

Figure S3 : Northern blotting of Gimap3 in spleen and thymus of Gimap5 wildtype and knockout mice.

15 ug of total RNA from each tissues and 5 ug for the cell line control was separated on formaldehyde gel and transfered to a charged nylon membrane followed by U.V. cross-linking. Oligonucleotide probes were end-labeled with ^{32}P-ATP then hybridized overnight with the membrane.

Files S1-S2

Available for download as Excel files at http://www.genetics.org/lookup/suppl/doi:10.1534/genetics.115.175596/-/DC1

FileS1 Complete LC-MS/MS data analysis

FileS2 List of proteins from iTRAQ LC-MS/MS